

Roquin-2 Shares Functions with Its Paralog Roquin-1 in the Repression of mRNAs Controlling T Follicular Helper Cells and Systemic Inflammation

Alvin Pratama,^{1,5} Roybel R. Ramiscal,^{1,5} Diego G. Silva,^{1,5} Souvik K. Das,¹ Vicki Athanasopoulos,¹ Jessica Fitch,¹ Natalia K. Botelho,¹ Peh-Ping Chang,¹ Xin Hu,¹ Jennifer J. Hogan,¹ Paula Maña,¹ David Bernal,¹ Heinrich Korner,⁴ Di Yu,¹ Christopher C. Goodnow,² Matthew C. Cook,^{2,3} and Carola G. Vinuesa^{1,*}

¹Department of Pathogens and Immunity

²Department of Immunology

³ANU Medical School

John Curtin School of Medical Research, Australian National University, Canberra, ACT 0200, Australia

⁴Cellular Immunology, Menzies Research Institute, Hobart, Tasmania 7000, Australia

⁵These authors contributed equally to this study

*Correspondence: carola.vinuesa@anu.edu.au

<http://dx.doi.org/10.1016/j.immuni.2013.01.011>

SUMMARY

Accumulation of T follicular helper (Tfh) cells and proinflammatory cytokines drive autoantibody-mediated diseases. The RNA-binding protein Roquin-1 (*Rc3h1*) represses the inducible costimulator ICOS and interferon- γ (IFN- γ) in T cells to prevent Tfh cell accumulation. Unlike *Rc3h1*^{san} mice with a mutation in the ROQ domain of Roquin-1, mice lacking the protein, paradoxically do not display increased Tfh cells. Here we have analyzed mice with mutations that eliminate the RING domain from Roquin-1 or its paralog, Roquin-2 (*Rc3h2*). RING or ROQ mutations both disrupted *Icos* mRNA regulation by Roquin-1, but, unlike the ROQ mutant that still occupied mRNA-regulating stress granules, RING-deficient Roquin-1 failed to localize to stress granules and allowed Roquin-2 to compensate in the repression of ICOS and Tfh cells. These paralogs also targeted tumor necrosis factor (TNF) in nonlymphoid cells, ameliorating autoantibody-induced arthritis. The Roquin family emerges as a posttranscriptional brake in the adaptive and innate phases of antibody responses.

INTRODUCTION

Roquin-1 is a RING (really interesting new gene)-domain containing protein encoded by the *Rc3h1* gene with an important function in controlling T follicular helper (Tfh) cells. It was discovered and revealed as a crucial regulator of self-tolerance when homozygosity for the *Rc3h1* “san” allele in mice, which causes an M199R amino acid substitution within a unique ROQ domain of the protein, was found to segregate with excessive formation of Tfh cells, spontaneous autoantibody production, and end-organ pathology typical of lupus (Vinuesa et al., 2005). Roquin-1 is expressed ubiquitously, but little is known about its other cellular actions, including those within the innate immune system.

Roquin-1 binds messenger RNA (mRNA) targets such as *Icos* promoting their decay through the ROQ domain and an adjacent CCCH-type zinc finger (Athanasopoulos et al., 2010; Chang et al., 2012; Glasmacher et al., 2010; Yu et al., 2007). Consistent with this function, Roquin-1 localizes to cytoplasmic stress granules (SGs) and processing (P) bodies, forming part of the mRNA decapping complex within P bodies through its ability to interact with RCK and the enhancer of decapping EDC4 (Glasmacher et al., 2010). In *Rc3h1*^{san/san} mice, the mutant protein fails to repress target mRNAs, leading to overexpression of the T cell inducible costimulator (ICOS) and interferon- γ (IFN- γ) (Lee et al., 2012; Yu et al., 2007). Both of these molecules contribute to the accumulation of Tfh cells that sustain and aberrantly select germinal center (GC) B cells and cause autoimmunity (Lee et al., 2012; Linterman et al., 2009; Yu et al., 2007).

Unlike *Rc3h1*^{san/san} mice, *Rc3h1*-null mice showed no accumulation of effector CD4⁺ T cells or Tfh cells (Bertossi et al., 2011), suggesting the possibility of the existence of a related protein with redundant functions. A family of *Rc3h1*-like genes and proteins can be traced in evolution from mammals to invertebrates. While *C. elegans* and *D. melanogaster* have a single ancestral gene, in humans and mice there is one clear Roquin-1 paralog, Roquin-2 (also known as MNAB, membrane-associated nucleic acid binding protein [Siess et al., 2000]). Roquin-2 is encoded by the *Rc3h2* gene. The two paralogs—Roquin-1 and Roquin-2—appear to have arisen by ancient gene duplication and lie on different chromosomes. The N termini of Roquin-1 and Roquin-2 share high-sequence similarity across the RING, ROQ, and CCCH (C3H) domains (Figure 1A). Although the function of Roquin-2 remains unknown, both Roquin-1 and Roquin-2 are expressed ubiquitously and localize to RNA-regulating SGs (Athanasopoulos et al., 2010). If the function of Roquin-1 can be shared by another protein, Roquin-2 is an obvious candidate.

Here we set out to investigate the function of Roquin-2 and possible functional redundancies between Roquin-1 and Roquin-2 by analyzing single- and double-RING mutant mice. The experiments reveal that these paralogs share overlapping mRNA targets and Roquin-2 can compensate for Roquin-1's RNA repression activity when Roquin-1 is not localized in SGs. These results also identify anti-inflammatory effects of the

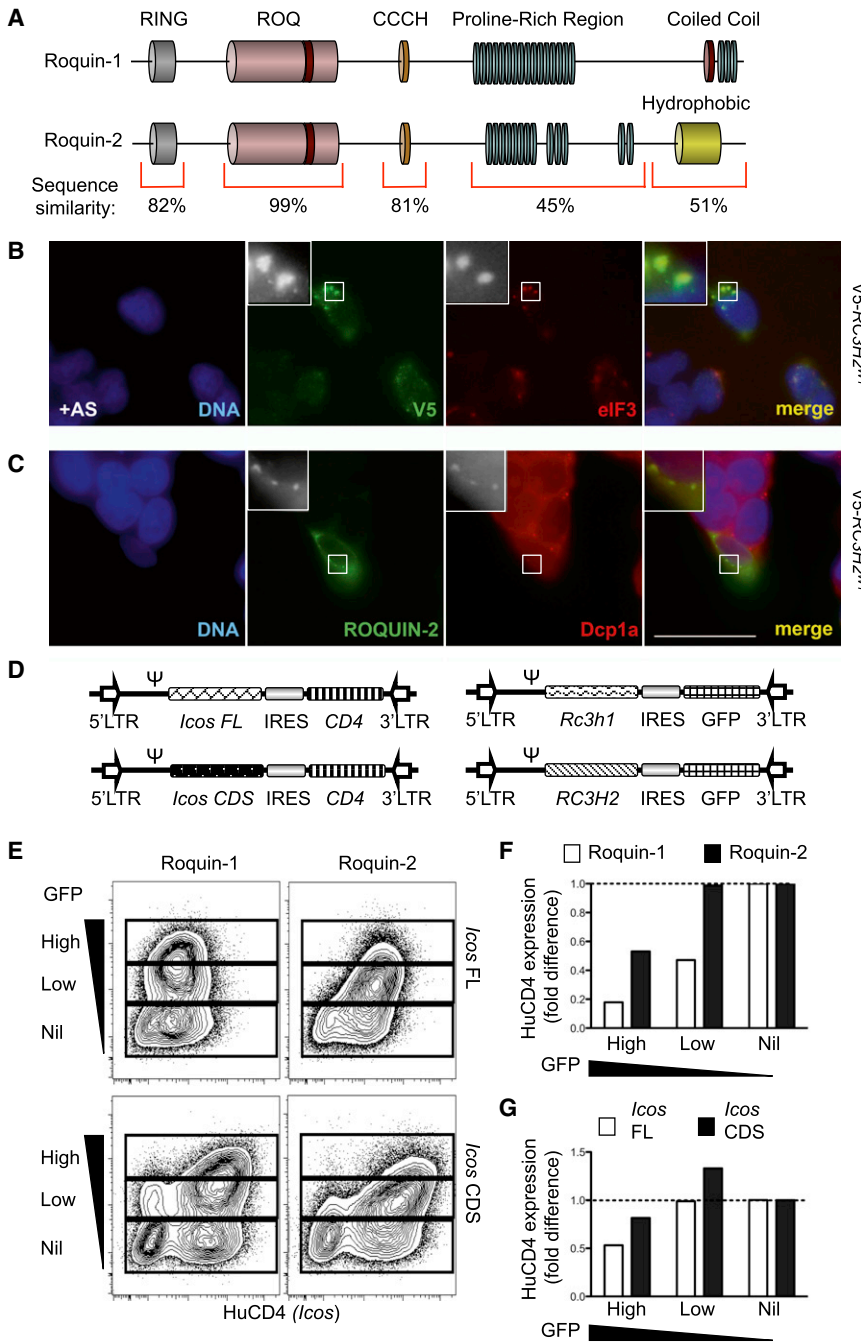


Figure 1. Roquin-2 Localizes to SGs and P Bodies and Represses *Icos* mRNA

(A) Schematic diagram of Roquin-1 and Roquin-2 proteins and amino acid sequence similarity for each domain.

(B and C) HEK293T cells were transfected with V5-RC3H2^{WT} (shown in green), treated with 1 mM sodium arsenite for 1 hr to induce SG formation, and then fixed and stained with anti-eIF3 (B) or anti-DCP1A (C) antibody (red). DNA is stained with 4',6-diamidino-2-phenylindole (blue). Images in (B) and (C) were all taken at the same magnification, and the scale bar represents 50 μ m.

(D) Retroviral vectors used to investigate full-length (FL) *Icos* mRNA (including coding sequence [CDS] and 3'UTR) and *Icos* CDS repression by Roquin-1 and Roquin-2. LTR, long terminal repeats; Ψ , retroviral packaging element; HuCD4, human CD4 protein; GFP, green fluorescent protein; IRES, internal ribosome entry site.

(E) Flow cytometric analysis of NIH 3T3 cells following retroviral cotransduction of *Rc3h1* (left panel) or *RC3H2* (right panel) with either *Icos* FL mRNA (top panel) or *Icos* CDS mRNA (bottom panel). Expression of Roquin-1 or Roquin-2 is assessed by GFP fluorescence, whereas that of ICOS is assessed by human CD4 (HuCD4) reporter.

(F) Quantification of HuCD4 (normalized to empty vector) on NIH 3T3 cells cotransduced with *Icos* FL mRNA and either *Rc3h1* or *RC3H2*. (G) Similar to (F), but NIH 3T3 cells were cotransduced with *RC3H2* and either *Icos* FL mRNA or *Icos* CDS mRNA. The vertical axes in (F) and (G) show the fold difference in HuCD4 expression on NIH 3T3 cells transduced with either *Rc3h1* or *RC3H2* relative to empty vector. The dashed lines in (F) and (G) indicate full (unrepressed) expression of HuCD4. Data are representative of three independent experiments. See also Figure S1.

SGs and P bodies, we tested whether Roquin-2 could also be found in these subcellular compartments. A complementary DNA (cDNA) encoding Roquin-2 was fused to a V5 tag and introduced into HEK293T cells. Staining cells for the SG and P-body markers eIF3 and DCP1A, respectively, revealed that Roquin-2 localized within both SGs (Figure 1B) and P bodies (Figure 1C) upon arsenite treatment.

products of these gene paralogs in nonlymphoid cells and establish a central role for the RC3H family as regulators of Tfh cell homeostasis and inflammatory disease.

RESULTS

Roquin-2 Localizes to Stress Granules and Represses *Icos* mRNA

Given the striking sequence similarity between Roquin-1 and Roquin-2 (Figure 1A), we hypothesized that they might have similar functions. Because Roquin-1 localizes to cytoplasmic

We next asked whether Roquin-2 could repress *Icos* mRNA, a target of Roquin-1. Roquin-2 and Roquin-1 were expressed in NIH 3T3 cells using *pR-IRES-GFP* retroviral vectors, together with a *pR-IRES-CD4* retroviral vector expressing either full-length (FL) *Icos* or only the coding region sequence (CDS), thus lacking the 3'UTR sequences recognized by Roquin-1 (Figure 1D). In this system, cell to cell differences in Roquin-1 and Roquin-2 expression are inferred from differences in GFP fluorescence, since they are encoded by a single bicistronic mRNA, and human CD4 (HuCD4) fluorescence is an indicator of *Icos* mRNA expression within individual cells. When NIH 3T3

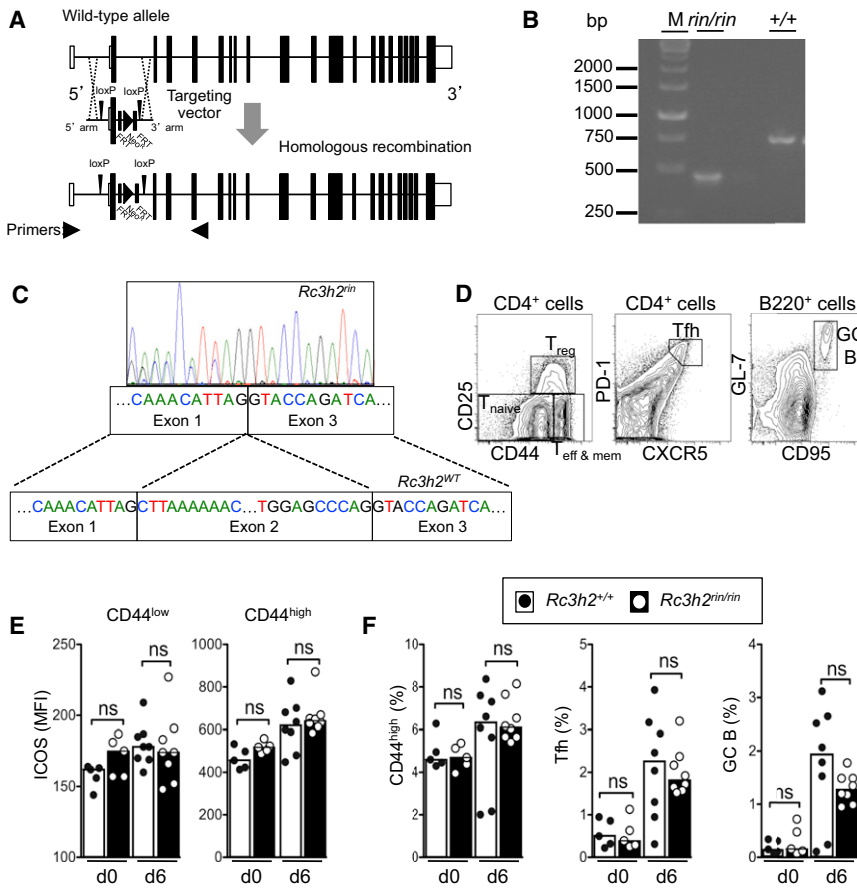


Figure 2. Generation and Phenotype of Roquin-2 RING-Deficient Mice

(A) Generation of Roquin-2 *ringless* mice with a deletion of *Rc3h2* exon 2 when crossed to *Rosa26-cre* transgenic strain. White boxes, noncoding exons; black boxes, protein encoding exons; Neo^R, Neomycin resistance cassette.

(B and C) Deletion of *Rc3h2* exon 2 detected in MEFs by PCR (B) and sequencing (C) from cDNA. Position of primers used for the PCR in (B) is indicated as arrowheads in (A). M, DNA marker; bp, base pairs; +/+, *Rc3h2*^{+/+}; *rin/rin*, *Rc3h2*^{rin/rin}. (D) Contour plots showing the gating strategy to isolate naive (CD44^{lo}), effector and memory (CD44^{hi}), and T_{reg} (CD25^{hi}) cells gated on CD4⁺ T cells (left panel), Tfh (CXCR5^{hi} PD-1^{hi}) cells gated on CD4⁺ T cells (middle panel), and GC B (CD95⁺ GL-7⁺) cells gated on B220⁺ cells (right panel).

(E) ICOS mean fluorescence intensity (MFI) on naive (CD44^{lo}, left panel) or effector and memory (CD44^{hi}, right panel) CD4⁺ T cells from mice sufficient (*Rc3h2*^{+/+}) or deficient (*Rc3h2*^{rin/rin}) in the Roquin-2 RING domain.

(F) Proportions of effector and memory (CD44^{hi}) cells (left panel) and Tfh (CXCR5^{hi} PD-1^{hi}) cells (middle panel) among total CD4⁺ T cells and of GC B cells among total B220⁺ cells (right panel) in *Rc3h2*^{+/+} and *Rc3h2*^{rin/rin} mice. (E–F) Percentages before (d0) and 6 days after SRBC immunization (d6) are shown. ns, not significant. Each dot represents an individual mouse and bars represent median values in each group. Data are representative of two independent experiments.

cells were cotransduced with *RC3H2-IRES-GFP* and *Icos FL-IRES-CD4*, cells expressing high amounts of *RC3H2-IRES-GFP* repressed HuCD4 expression by ~50%, indicating that Roquin-2 represses *Icos* 3'UTR mRNA, albeit possibly to a lesser extent than Roquin-1 (Figures 1E and 1F). As shown previously for Roquin-1, Roquin-2 did not repress *Icos* mRNA in cells transduced with *Icos CDS-IRES-CD4* (Figures 1E and 1G), suggesting that mRNA repression by Roquin-2 occurs via 3'UTR targeting. We considered the possibility that Roquin-1 and Roquin-2 form dimers or interact to jointly repress shared mRNA targets. Reciprocal coimmunoprecipitation of Roquin-1-FLAG and V5-Roquin-2 ectopically expressed in HEK293T cells failed to reveal an interaction between Roquin-1 and Roquin-2 (see Figure S1 available online). Collectively, these data indicate that Roquin-2 and Roquin-1 have independent, overlapping ability to destabilize *Icos* mRNA when their expression is enforced in vitro.

In Vivo Targeted Deletion of the Roquin-1 and Roquin-2 RING Domains

To compare the role of Roquin-1 and Roquin-2 as regulators of mRNA decay in vivo, we used gene targeting in mice to produce loss-of-function mutations that eliminated the RING domain from Roquin-1 or Roquin-2. The *cre-LoxP* methods were used to ablate *Rc3h2* exon 2, encoding the Roquin-2 translation start site and RING domain, upon crosses with *Rosa26-cre* transgenic mice to generate a germline deficiency (Figure 2A). This allele has been designated *Rc3h2*^{rin}. In the resulting *Rc3h2*^{rin} mRNA, skip-

ping of exon 2 resulted in a smaller transcript due to splicing of exon 1 to exon 3 (Figures 2B and 2C), yielding an alternative in-frame Kozak translation initiation site at Met130. Homozygous *Rc3h2*^{rin/rin} mice, which lacked the Roquin-2 RING domain in all cell types, were viable and did not display ICOS overexpression (Figures 2D and 2E). Enumeration of effector and memory CD4⁺, Tfh, and GC B cells before or 6 days after sheep red blood cells (SRBC) immunization did not reveal any differences with control mice (Figures 2D and 2F).

The same strategy was used to produce mice with a germline or T cell-specific deletion of *Rc3h1* exon 2, which encodes the Roquin-1 translation start codon and RING domain. Like the *Rc3h2*^{rin} allele, the resulting *Rc3h1 ringless* (*Rc3h1*^{rin}) mRNA also splices exon 1 to exon 3, yielding an alternative in-frame Kozak translation initiation site at Met133 that produces an N-terminally truncated protein. Homozygosity for the germline *Rc3h1*^{rin} results in perinatal lethality and a phenotype similar to that described in mice lacking *Rc3h1*, with a lung inflation defect and an incomplete closure of the neural tube (Figures 3A and 3B). The phenotypic similarity between *Rc3h1*^{rin/rin} and *Rc3h1*^{-/-} suggests that the *Rc3h1*^{rin} allele results in a severe loss of function (Bertossi et al., 2011).

To circumvent perinatal lethality and investigate the consequences of the *Rc3h1*^{rin} mutation on ICOS regulation in T cells, we generated mice with a T cell-specific deletion of Roquin-1 RING (*Rc3h1*^{fllox/fllox} *Lck-cre*). As in mice lacking *Rc3h1* (Bertossi et al., 2011), there was no spontaneous accumulation of Tfh cells

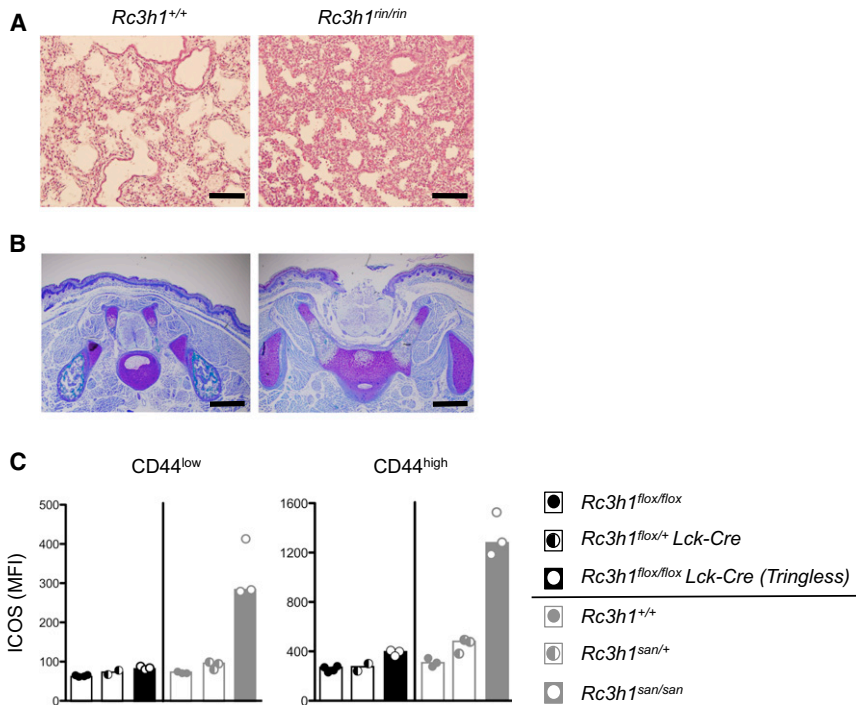


Figure 3. Roquin-1 RING Deficiency Causes Perinatal Mortality but Minimally Impairs ICOS Repression

(A and B) Histological assessments of lung by hematoxylin and eosin (H&E) staining (A) and lumbar neural tube by Luxol Fast Blue-Cresyl Violet (LFB-CV) staining (B) of embryos sufficient (*Rc3h1*^{+/+}) (left panel) or deficient (*Rc3h1*^{rin/rin}) (right panel) in the Roquin-1 RING at embryonic day 19 (E19). Scale bar on the lung photomicrograph (A) represents 100 μ m and that on the vertebrae photomicrograph (B) represents 500 μ m. (C) ICOS MFI on naive (CD44^{lo}) or effector and memory (CD44^{hi}) CD4⁺ T cells from mice with T cell conditional deletion of *Rc3h1* RING (*Rc3h1*^{flox/flox} *Lck-cre*) or littermate controls (*Rc3h1*^{flox/+} *Lck-cre* and *Rc3h1*^{flox/flox}) and from mice with the Roquin-1 M199R (ROQ) point mutation (*Rc3h1*^{san/san}) or littermate controls (*Rc3h1*^{san/+} and *Rc3h1*^{+/+}). Each dot represents an individual mouse and bars represent the median value in each group. See also Figure S2.

in *Rc3h1*^{flox/flox} *Lck-cre* (*Tringless*) mice; GC B cell numbers were comparable to those of *Rc3h1*^{flox/flox} mice (data not shown). ICOS expression on naive (CD44^{lo}) and effector and memory (CD44^{hi}) CD4⁺ T cells was increased slightly in Roquin-1 *Tringless* mice similar to mice heterozygous for the *Rc3h1*^{san} allele analyzed in parallel (Figure 3C) but much less than in homozygous *Rc3h1*^{san/san} mice (Figure 3C).

Roquin-2 Compensates for RING-Deficient Roquin-1

We next tested the possibility that the apparent loss of function of Roquin-1^{RINGLESS} protein allowed its *Icos*-regulating function to be compensated by wild-type (WT) Roquin-2 in Roquin-1 *Tringless* mice. Supporting this hypothesis, Roquin-2 was found to localize normally to SGs in *Rc3h1*^{rin/rin} mouse embryonic fibroblasts (Figures S2A and S2B). The RING domains were ablated from both Roquin-1 and Roquin-2 in T cells by breeding *Lck-cre* transgenic mice bearing homozygous *Rc3h1*^{flox/flox} and *Rc3h2*^{flox/flox} alleles. Double Roquin-1 and Roquin-2 *Tringless* mice (*Rc3h1*^{flox/flox} *Rc3h2*^{flox/flox} *Lck-cre*) had elevated ICOS expression on effector and memory (CD44^{hi}) CD4⁺ and Tfh (CXCR5^{hi} PD-1^{hi}) cells compared to control *Rc3h1*^{flox/flox} *Rc3h2*^{flox/flox} mice that did not inherit the *Lck-cre* transgene or to their single *Tringless* counterparts (Figure 4A). This was accompanied by increased IFN- γ -producing cells and increased formation of Tfh and GC B cells upon SRBC immunization (Figures 4A and 4B). Nevertheless, ICOS expression and Tfh and GC B cell numbers were still higher in *Rc3h1*^{san/san} mice than in double Roquin-1 and Roquin-2 *Tringless* mice (Figure 4B).

Deletion of the RING Domain Affects Localization to SGs

The data above suggest that Roquin-2 can compensate for Roquin-1^{RINGLESS} but not Roquin-1^{SAN} mutations. There are two possible interpretations for this difference. First, the “san”

missense mutation is either a neomorphic or antimorphic allele, where the M199R substitution results in a protein with novel or dominant-negative activity. To test whether the requirement for homozygosity of the *Rc3h1*^{san} allele was due to a gain-of-function or antimorphic effect that only occurred with a double gene dosage of point mutant protein, we compared mice that carried a single copy of the *Rc3h1*^{san} allele but carried, on the other chromosome, either a normal *Rc3h1* gene (*san/+*) or the loss-of-function *Rc3h1*^{rin} allele (*san/rin*). T cells in the resulting compound heterozygous *Rc3h1*^{san/rin} mice displayed increased CD44^{hi} CD4⁺ and Tfh cells and exaggerated ICOS expression on naive CD4⁺ cells comparable to T cells from *Rc3h1*^{san/san} mice with a double genetic dose of the point mutant protein (Figure 4C). This result indicates that the recessive ICOS dysregulation caused by *Rc3h1*^{san} reflects a loss of Roquin-1’s RNA-regulating function.

The second interpretation for the inability of Roquin-2 to compensate for Roquin-1^{SAN} is that the “san” allele may act recessively to encode a “niche-filling” protein, where assembly into the mRNA regulating complex is preserved but the normal mRNA-repressing function of Roquin-1 is lost. Previous evidence has been presented that Roquin-1^{SAN} localizes normally to SGs (Athanasopoulos et al., 2010). Repression of mRNAs such as *Icos* by Roquin-1 correlates with localization of the protein to cytoplasmic P bodies, subcellular cytoplasmic compartments where 5’-3’ mRNA decay is thought largely to occur (Glasmacher et al., 2010). P bodies and SGs have been shown to be dynamically linked structures and their fusion promoted and even stabilized by RNA-binding proteins such as TTP and BRF1 (Kedersha et al., 2005). Localization of Roquin-1^{SAN} in the correct niche could then prevent compensatory substitution by related proteins with overlapping functions. This type of compensation for null but not missense alleles has previously been demonstrated for the IKAROS protein family (Papathanasiou et al., 2003). We therefore looked at the ability of an N-terminal RING domain deleted Roquin-1 (Roquin-1¹³³⁻¹¹³⁰;

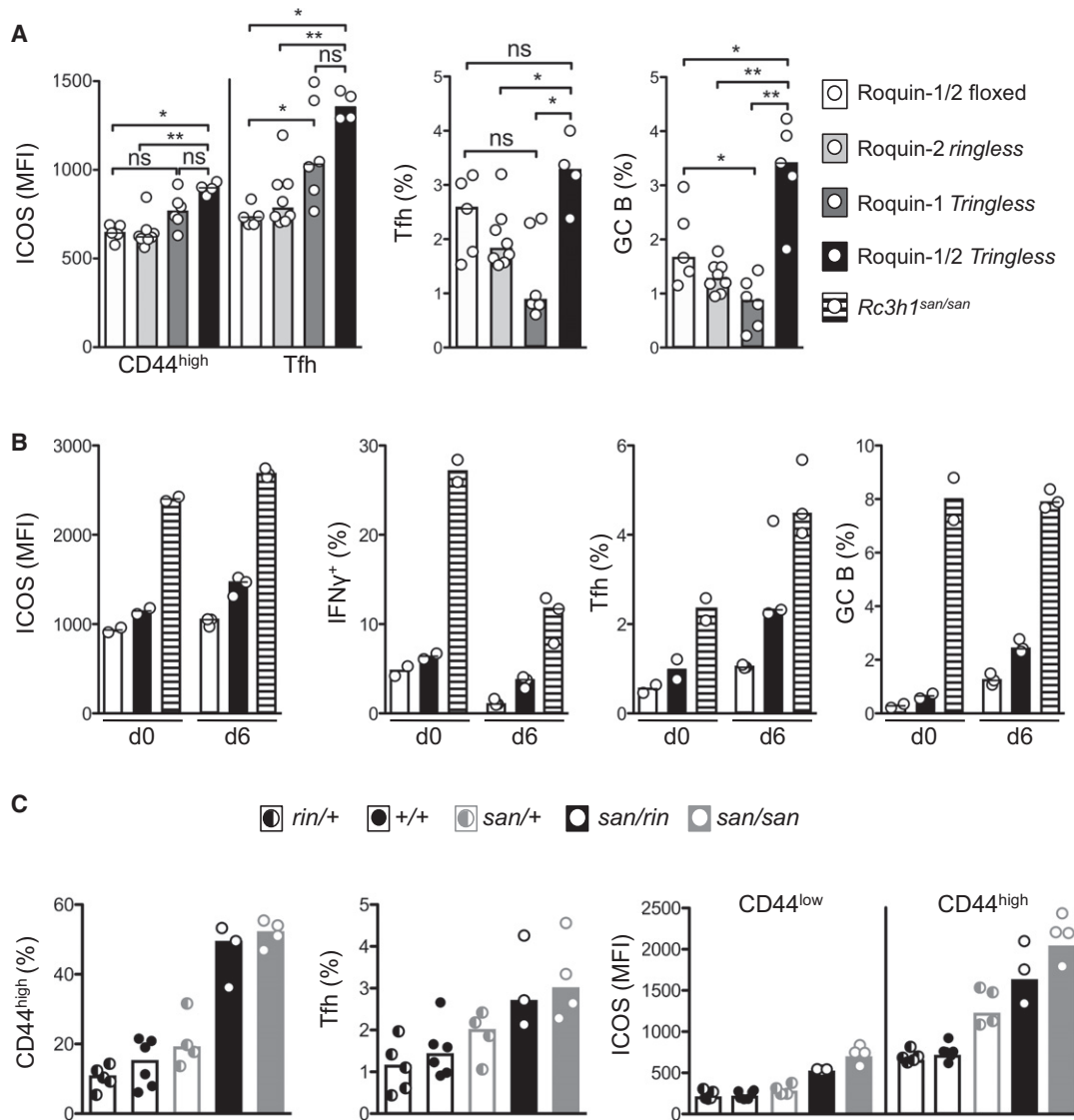


Figure 4. Partially Overlapping Functions of Roquin-1 and Roquin-2 in the Repression of Tfh Cell Activity and Inflammation

(A) Flow cytometric analysis on *Lck-cre* expressing double *Rc3h1* and *Rc3h2*-floxed (Roquin-1 and Roquin-2 *Tringless*) mice and controls examined 6 days post-SRBC immunization showing ICOS MFI on effector and memory (CD44^{hi}) and Tfh (CXCR5^{hi} PD-1^{hi}) CD4⁺ T cells and proportions of Tfh cells among total CD4⁺ T cells and GC B among total B220⁺ cells. Control groups include double Roquin-1 and Roquin-2 floxed (*Rc3h1*^{fllox/fllox} *Rc3h2*^{fllox/fllox}), *Rc3h2*^{rin/rin} (Roquin-2 *ringless*) and *Rc3h1*^{fllox/fllox} *Lck-cre* (Roquin-1 *Tringless*) mice. *p ≤ 0.05; **p ≤ 0.01; ***p ≤ 0.001. Data are representative of two independent experiments.

(B) Flow cytometric analysis on the double RING-domain mutant (Roquin-1 and Roquin-2 *Tringless*) mice and the Roquin-1 ROQ-domain mutant (*Rc3h1*^{san/san}) mice, showing ICOS MFI on Tfh (CXCR5^{hi} PD-1^{hi}) cells, proportions of IFN- γ ⁺ cells and Tfh (CXCR5^{hi} PD-1^{hi}) cells among total CD4⁺ T cells and proportions of GC B cells among total B220⁺ cells. Percentages before (d0) and 6 days after SRBC immunization (d6) are shown.

(C) Proportions of effector and memory (CD44^{hi}) cells (left panel) and Tfh (CXCR5^{hi} PD-1^{hi}) cells (middle panel) among total CD4⁺ T cells and ICOS MFI on naive (CD44^{lo}) or effector and memory (CD44^{hi}) CD4⁺ T cells (right panel) from *Rc3h1*^{+/+}, *Rc3h1*^{rin/+}, *Rc3h1*^{san/+}, *Rc3h1*^{san/rin}, and *Rc3h1*^{san/san} mice. Data are pooled from two experiments. Each dot represents an individual mouse and bars represent the median value in each group.

Roquin-1^{RINGLESS}) to localize to P bodies and to SGs. When ectopically expressed in HEK293T cells, V5-tagged Roquin-1^{RINGLESS} was still able to localize to P bodies, but only colocalized with eIF3 (a SG marker) in 5% of arsenite-treated cells compared to Roquin-1^{WT}, which colocalized with eIF3 in 91% of stressed cells (Figures 5A–5D). Additional tests using a different marker for SG colocalization, TIA-1, confirmed that Roquin-1^{RINGLESS} localized outside of, but adjacent to, SGs (Fig-

ures S3A–S3B'). Even though Roquin-2 still localized to SGs in the presence of Roquin-1^{SAN} (Figures S3C–S3E), the latter, although not functional, is likely to retain its scaffold position within RNA granules. Thus, unlike Roquin-1^{RINGLESS}, Roquin-1^{SAN} may not create a void in the multimolecular RNA-regulating assembly in SGs for Roquin-2 to occupy (Figure S3F).

Given our previous observation that GFP-tagged fragments of Roquin-1 (138–337 or 138–484) that lacked both the RING

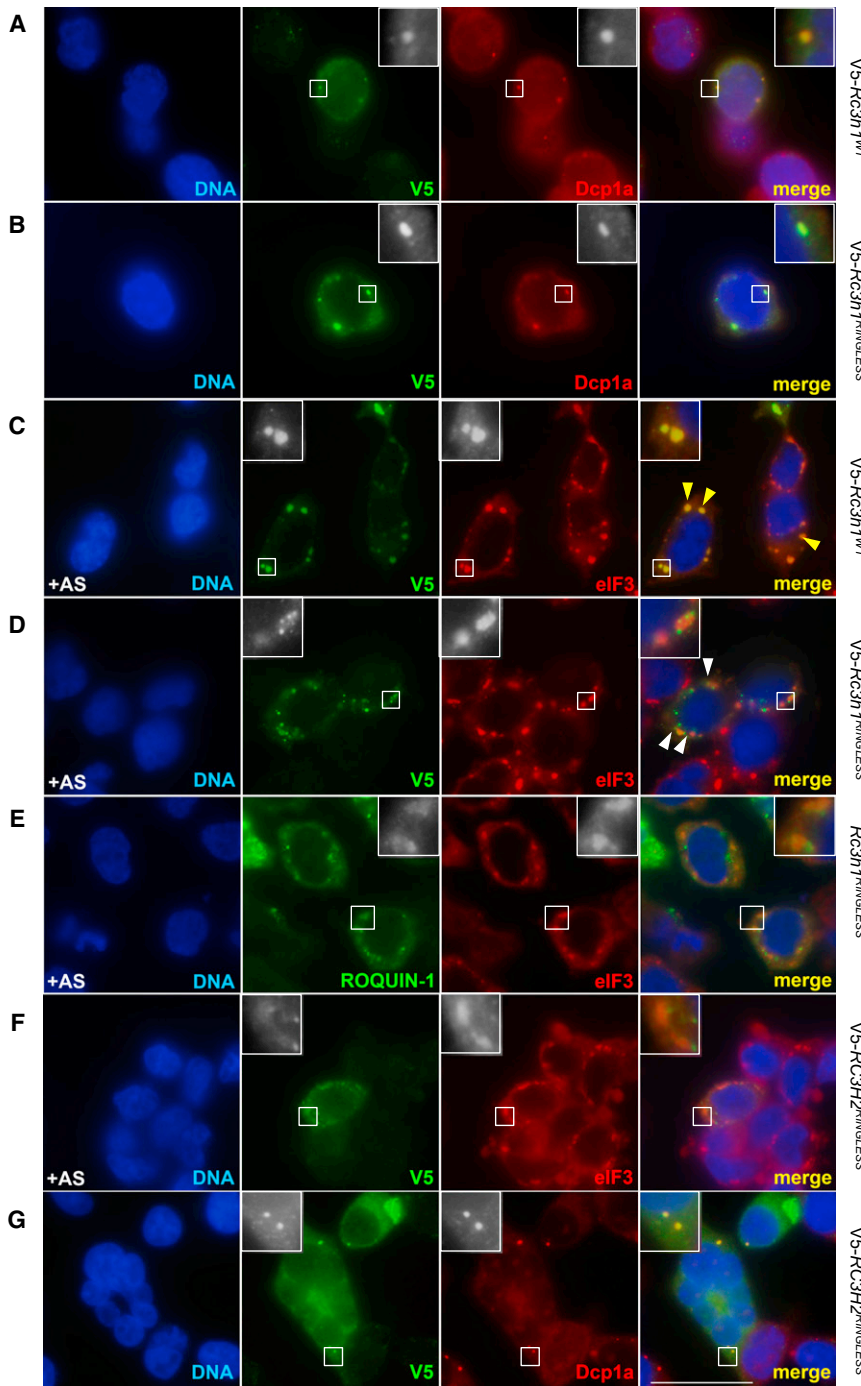


Figure 5. Deficiency in the RING Domain Causes Impaired SG Localization

(A and B) HEK293T cells transfected with V5-*Rc3h1*^{WT} (A) and V5-*Rc3h1*^{RINGLESS} (B) were fixed and costained with V5 antibody (green) and the P body (PB) marker DCP1A (red).

(C–E) HEK293T cells were transfected with V5-*Rc3h1*^{WT} (C), V5-*Rc3h1*^{RINGLESS} (D), or untagged *Rc3h1*^{RINGLESS} (E), treated with 1 mM sodium arsenite for 1 hr to induce SG formation. Cells were fixed and stained with eIF3 antibody (shown in red) and either V5 antibody (green in C and D), or a Roquin-1-specific antibody (green in E). Ectopically expressed V5-*Rc3h1*^{WT} localizes to eIF3⁺ SGs (yellow arrowheads). White arrowheads show V5-*Rc3h1*^{RINGLESS} with impaired localization to eIF3⁺ granules.

(F) HEK293T cells were transfected with V5-*RC3H2*^{RINGLESS} (stained with anti-V5, green), treated with 1 mM sodium arsenite for 1 hr to induce SG formation (+AS), then fixed and stained with anti-eIF3 (shown in red).

(G) Nonstressed transfected cells were stained with anti-DCP1A antibody (red). Images in (A)–(G) were all taken at the same magnification, and the scale bar represents 50 μm. Boxed inserts magnify one particular region. DNA is stained with 4',6-diamidino-2-phenylindole (blue). See also Figure S3.

tion engineered in the mice, which selectively removes the RING domain from an otherwise full-length protein, results in a failure of the protein to localize to SGs.

Roquin-2 RING Deficiency Exacerbates Roquin-1^{SAN} Lethality and Immune Pathology

In order to further understand the functional overlap between the two Roquin proteins and also test whether there are any unique functions of Roquin-2, we examined the effects of Roquin-2 RING deficiency on the pathology caused by homozygous *Rc3h1*^{san/san} mutation. *Rc3h1*^{san/san} mice were crossed to *Rc3h2*^{rin/rin} mice to generate *Rc3h1*^{san/san} *Rc3h2*^{rin/rin} mice and the relevant littermate controls. Roquin-2 RING deficiency caused premature and fully penetrant mortality of *Rc3h1*^{san/san} mice, with no mice surviving beyond 22 weeks (Fig-

ure 6A). Examination of the double-mutant mice revealed elevated percentages of Tfh cells (Figure S4A) and more severe inflammatory infiltrates in the kidney (Figure 6B) and other organs (data not shown). Double mutant mice also exhibited increased susceptibility to low-dose lipopolysaccharide (LPS): 2.5 μg/g body weight LPS injection was lethal for 3 out of 4 double mutants, but all single mutant controls survived; serum tumor necrosis factor (TNF) in the surviving mouse 72 hr postinjection was 100-fold higher than in the controls (Figure S4B). Similar susceptibility to LPS was also observed in irradiated

domain and the C-terminal half of the protein could localize to SGs (Athanasopoulos et al., 2010), we investigated the possibility that the altered localization of the Roquin-1^{RINGLESS} (133–1130) mutant studied here was related to the tag. Retrovirally expressed untagged Roquin-1^{RINGLESS} (133–1130) also failed to localize to SGs (Figure 5E) in HEK293T cells. Similar to Roquin-1^{RINGLESS}, the RING-deficient Roquin-2 protein (Roquin-2^{RINGLESS}) localized outside SGs upon stress induction (Figure 5F) but retained its normal P-body localization (Figure 5G). These results conclusively demonstrate that the muta-

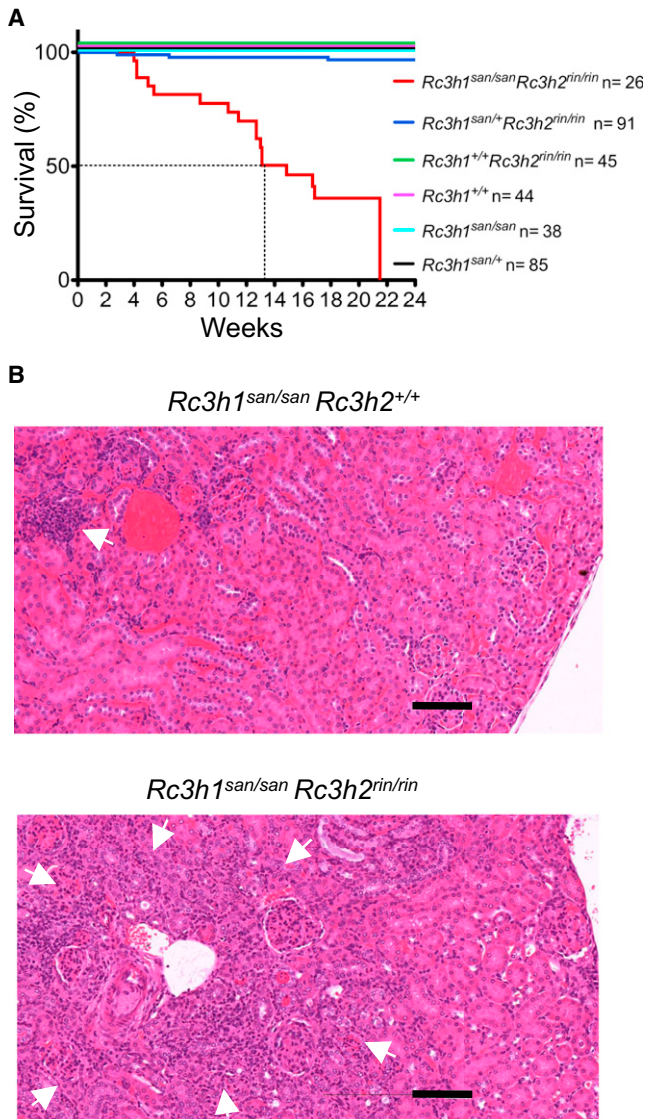


Figure 6. RING Deficiency in Roquin-2 Causes Early Lethality and Exacerbated Tissue Damage in *Rc3h1^{san/san}* Mice

(A) Survival curve of weaned *Rc3h1^{san/san} Rc3h2^{rin/rin}* double-mutant mice and control littermates with the indicated genotypes. (B) H&E stains of kidneys from 13-week-old *Rc3h1^{san/san}* (top panel) and *Rc3h1^{san/san} Rc3h2^{rin/rin}* (bottom panel) mice. Arrows indicate tissue infiltrates. Scale bar represents 100 μ m. See also Figure S4.

Rag1^{-/-} recipient mice transplanted with *Rc3h1^{san/san} Rc3h2^{rin/rin}* bone marrow: 1.2 μ g/g body weight LPS was lethal in 4 out of 5 mice, whereas mice in single mutant control groups (*Rc3h1^{san/san}* and *Rc3h2^{rin/rin}*) remained healthy. These results suggested that Roquin-1 and Roquin-2 control production of proinflammatory cytokines.

Roquin-1 and Roquin-2 Act in Non-T Cells to Prevent TNF-Dependent Immune Pathology

Lethality to LPS is mediated by secretion of proinflammatory cytokines by macrophages. We found elevated TNF in the serum of *Rc3h1^{san/san}* mice compared to control littermates, whereas

interleukin-1 (IL-1) was undetectable (Figure 7A; data not shown). Given that the single ancestral *Roquin* gene is present in *C. elegans*, and the appearance of the two paralogs only occurs in jawed vertebrates after the appearance of adaptive immunity, we considered the possibility the Roquin paralogs may regulate innate immunity, specifically acting in myeloid cells to regulate TNF-mediated immunity. To investigate the role of Roquin-1 in nonlymphoid cells, we generated T and B cell-deficient *Rag1^{-/-} Rc3h1^{san/san}* and *Rag1^{-/-} Rc3h1^{+/+}* control mice. Whereas lethality to high doses of LPS is primarily mediated by secretion of IL-1 by macrophages (Ohlsson et al., 1990), low doses of LPS combined with D-galactosamine treatment cause lethal shock largely mediated by TNF because *Tnfrsf1a^{-/-}* mice are resistant to this challenge (Peschon et al., 1998). Whereas ten out of ten *Rag1^{-/-} Rc3h1^{+/+}* mice remained unaffected, six out of eight *Rag1^{-/-} Rc3h1^{san/san}* mice died from endotoxic shock within 24 hr of low-dose LPS (5 μ g/g) plus 20 mg D-galactosamine injection (Figure 7B).

We inferred from this finding that Roquin-1 and Roquin-2 might interact to regulate innate immunity and the inflammatory response in autoimmunity (in addition to CD4⁺ T cell responses). We investigated this further by using the K/BxN model of rheumatoid arthritis (Korganow et al., 1999; Matsumoto et al., 1999; Solomon et al., 2005), modified by the elimination of T and B cells. Joint inflammation in the K/BxN model is usually more dependent on IL-1 β than TNF (Ji et al., 2002), but arthritis in *Rag1^{-/-} Rc3h1^{san/san}* mice was accompanied by an exaggerated TNF response in lymph nodes draining arthritic joints (Figure 7C) and in macrophages isolated by peritoneal lavage; of note, systemic amounts of TNF did not increase (Figure S5A). Also, in contrast to the spontaneously elevated serum TNF observed above in *Rc3h1^{san/san}* mice with an intact T and B cell repertoire, baseline serum TNF was comparable between *Rag1^{-/-} Rc3h1^{san/san}* and *Rag1^{-/-} Rc3h1^{+/+}* mice (Figure S5B). *Rag1^{-/-} Rc3h1^{san/san}* exhibited heightened susceptibility to arthritogenic K/BxN serum compared to *Rag1^{-/-}* control mice (Figure 7D). Furthermore, a serum dose (50 μ l) that was subarthritogenic in most *Rag1^{-/-} Rc3h1^{+/+}* control mice induced severe arthritis in *Rag1^{-/-} Rc3h1^{san/san}* mice (Figure 7D). Synovial inflammation induced by passive transfer of 200 μ l K/BxN serum was also more pronounced in the joints of *Rag1^{-/-} Rc3h1^{san/san}* mice (Figure S5C), which contained large numbers of F4/80⁺ macrophages (Figure S5D). There was a small increase in *Il1b* mRNA (Figure 7C); nevertheless, TNF appears to account for the heightened susceptibility to arthritis in this model because the response serum in *Rag1^{-/-} Rc3h1^{san/san}* was rendered similar to that in *Rag1^{-/-}* mice by deletion of *Tnf* (Figure 7E).

After restimulation ex vivo with LPS, TNF production was 50-fold higher per cell in cultures of macrophages from *Rag1^{-/-} Rc3h1^{san/san}* mice compared to controls (Figures S5E and S5F). This was not the result of an increased number of myeloid cells because the expansion of the myeloid cell compartment seen in *Rag1^{+/+} Rc3h1^{san/san}* (Vinesa et al., 2005) mice is corrected in *Rag1^{-/-} Rc3h1^{san/san}* mice, and spleen cell counts in mutant and control littermates are comparable (Figure S5G). Collectively, these findings suggested that Roquin-1^{SAN} conferred an increased susceptibility to arthritis due to an incremental effect of TNF to pathology normally mediated by IL-1.

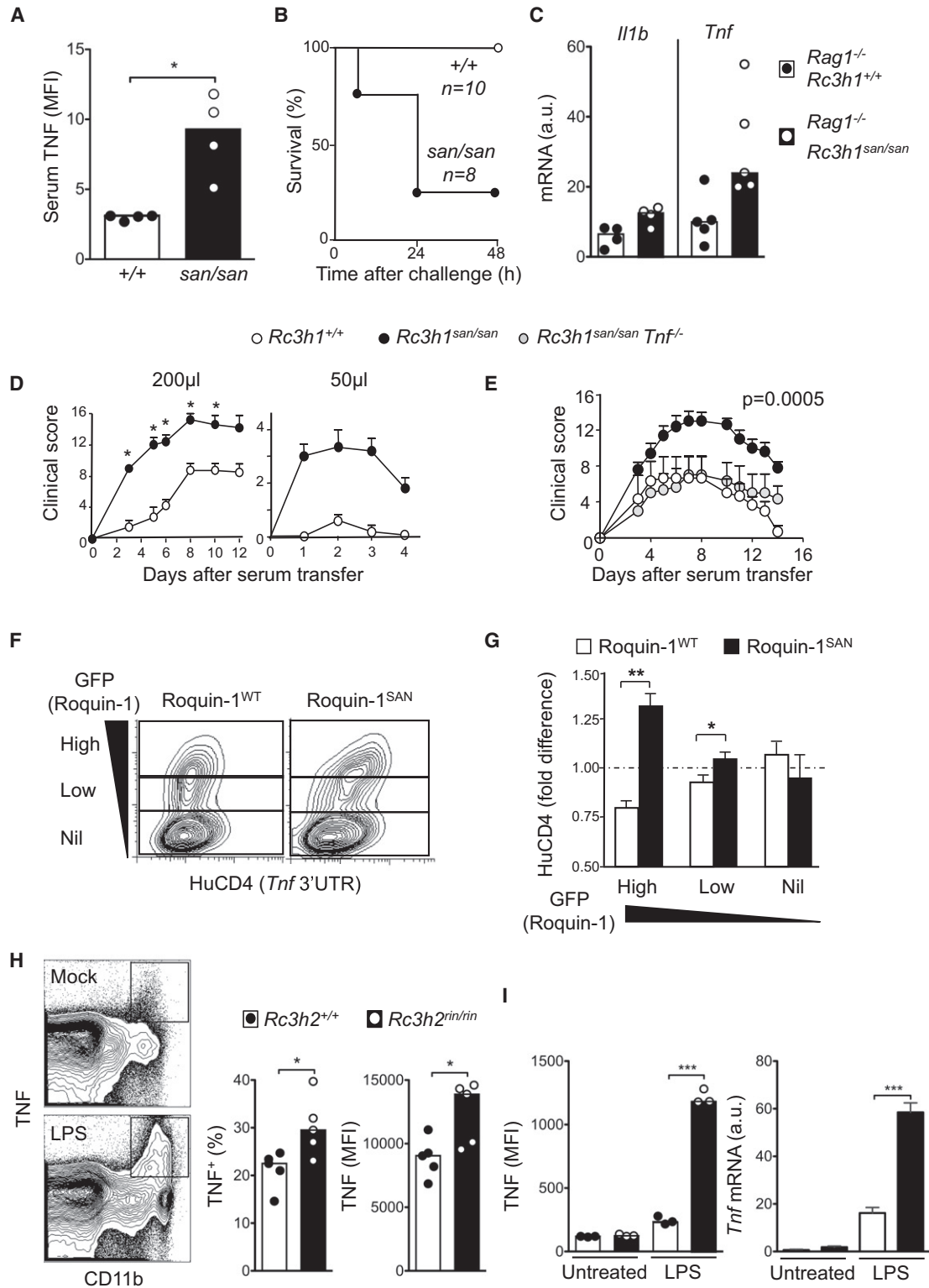


Figure 7. Roquin-1 and Roquin-2 Repress TNF and TNF-Mediated Pathology

(A) Serum TNF assessed by flow cytometric bead array (BD Biosciences) from *Rc3h1*^{+/+} and *Rc3h1*^{san/san} mice. Each dot represents an individual mouse and bars represent the median value in each group. *p ≤ 0.05.

(B) Survival curves for *Rag1*^{-/-} *Rc3h1*^{+/+} and *Rag1*^{-/-} *Rc3h1*^{san/san} mice after injection of LPS (5 µg/g) plus 20 mg D-gal (n = 8 and 10 per group, respectively).

(C) *Il1b* and *Tnf* transcripts found in draining lymph nodes of *Rag1*^{-/-} *Rc3h1*^{+/+} and *Rag1*^{-/-} *Rc3h1*^{san/san} mice 3 days after 50 µl K/BxN serum injection. Data expressed relative to β-actin in unfractionated popliteal lymph nodes. a.u., arbitrary unit.

(legend continued on next page)

In order to test the proposition that Roquin-1 represses TNF via a posttranscriptional mechanism similar to that described for *Icos* mRNA, WT Roquin-1 (Roquin-1^{WT}) and Roquin-1^{SAN} were expressed in NIH 3T3 cells by using the *pR-IRES-GFP* retroviral vectors described in Figure 1D, together with a *pR-IRES-CD4* retroviral vector expressing the 3'UTR of *Tnf*. When NIH 3T3 cells were cotransduced with *Rc3h1-IRES-GFP* and *Tnf 3'UTR-IRES-CD4*, cells expressing high amounts of Roquin-1 repressed HuCD4 expression by ~25% (Figures 7F and 7G), indicating that Roquin-1 represses *Tnf* 3'UTR mRNA. By contrast, cells transduced with *Rc3h1^{san}-IRES-GFP* and expressing high amounts of Roquin-1^{SAN} displayed a significant increase in HuCD4 expression (Figures 7F and 7G), consistent with the hypothesis that Roquin-1^{SAN} acts to promote *Tnf* mRNA stability via its 3'UTR.

To assess whether Roquin-2 has an independent role in regulating TNF, we investigated production of this cytokine in *Rc3h2^{rin/rin}* mice, which have intact Roquin-1. Upon intraperitoneal LPS (2.5 µg/g body weight) injection, there was an increased proportion of TNF-producing cells among CD11b⁺ macrophages (Figure 7H). TNF expression within splenic CD11b⁺ cells was also higher in *Rc3h2^{rin/rin}* mice compared to WT littermates (Figure 7H). In addition, Roquin-2 *ringless* MEFs were cultured with 10 µg/ml LPS and TNF secretion was measured: lack of Roquin-2 RING domain led to increased TNF production (Figure 7I). Roquin-2 *ringless* MEFs also expressed ~3-fold higher amounts of *Tnf* mRNA compared to controls (Figure 7I). Roquin-1 and Roquin-2 also appeared to regulate TNF production in CD4⁺ T cells because the proportion of TNF⁺ CD4⁺ T cells was increased in *Rc3h1^{san/san}* mice and double Roquin-1 and Roquin-2 *Tringless* mice following low-dose LPS, but not in single-mutant mice (Figure S5H). Together these results suggest that Roquin-1 and Roquin-2 have partially but not completely overlapping roles in TNF repression that are important to dampen endotoxic shock and autoantibody-dependent arthritis.

DISCUSSION

The experiments above illuminate the function of Roquin-1 and Roquin-2, showing that these evolutionarily paralogous proteins act in concert to dampen key mRNAs controlling inflammation

and autoimmunity, including a known Roquin-1 target *Icos* and an additional target, *Tnf*. Both Roquin proteins localize to mRNA-regulating SGs and P bodies in the cytoplasm, and both repressed *Icos* mRNA in a 3'UTR-dependent fashion in overexpression studies. The RING domain of both proteins is shown here to be critical for their localization to SGs and their function. In the absence of its RING domain, Roquin-1^{RINGLESS} protein behaved like a complete loss-of-function allele in causing perinatal lethality and vertebral malformations. Roquin-1^{RINGLESS} protein was also unable to complement the ROQ M199R point mutant protein to regulate *Icos* mRNA in T cells of compound heterozygous *Rc3h1^{san/rin}* mice. These in vivo results confirm overexpression data of Glasmacher et al. (2010) that showed a Roquin-1 construct lacking the RING domain had impaired ability to repress *Icos* mRNA in vitro, and establish that the ROQ M199R point mutation in the *Rc3h1^{san}* mice is also a loss-of-function allele with respect to *Icos* repression. WT Roquin-2, but not the *Rc3h2^{ringless}* allele, was able to compensate for loss of RING domain from Roquin-1 to control *Icos* mRNA in T cells. Loss of the RING domain from Roquin-2 on its own, exaggerated *Tnf* mRNA accumulation in response to LPS, and cooperated with the Roquin-1 M199R mutant to increase proinflammatory cytokines, organ inflammation, and mortality.

Our results provide evidence for overlapping functions of the two proteins because the phenotypes conferred by defects in Roquin-1 can be amplified by defects in Roquin-2. Because the *Rc3h1^{ringless}* mutation behaves like a Roquin-1 null allele with respect to perinatal lethality and pathology, this poses two key questions: (1) Why does *Rc3h1^{ringless}* cause so little dysregulation of ICOS or Tfh cells compared to the *Rc3h1^{san}* mutation, and (2) Why does the *Rc3h1^{san}* mutation not cause perinatal lethality? Analysis of compound heterozygous *Rc3h1^{san/rin}* mice revealed pronounced dysregulation of ICOS and CD4⁺ T cells, indicating that the RING and ROQ domain mutations each disrupt *Icos* mRNA repression. The two mutations nevertheless differ in their effects on SG localization, because this step is disrupted by the RING domain mutation but not the ROQ domain point mutation. The Roquin-1^{RINGLESS} mutant protein, but not the Roquin-1^{SAN} protein, vacates its subcellular niche within SGs; however, both proteins still localize to P bodies. As shown here, *Icos* repression is preserved in

(D) Arthritis clinical score of *Rag1^{-/-} Rc3h1^{+/+}* and *Rag1^{-/-} Rc3h1^{san/san}* after injection with 200 µl (left panel) or 50 µl (right panel) of K/BxN serum. Experiments were performed by using four or five mice per group for each dose. Data are representative of two independent experiments. Each dot represents mean arthritis score, and error bar represents SD; *p ≤ 0.05.

(E) Arthritis clinical score in *Rag1^{-/-} Rc3h1^{+/+}*, *Rag1^{-/-} Rc3h1^{san/san}*, and *Rag1^{-/-} Rc3h1^{san/san} Tnf^{-/-}* mice after transfer of 200 µl arthritogenic serum. Experiments were performed by using four and five mice per group. Each dot represents mean arthritis score, and error bar represents SD.

(F) Flow cytometric analysis of NIH 3T3 cells following retroviral cotransduction of *Rc3h1^{WT}* (left panel) or *Rc3h1^{SAN}* (right panel) with *Tnf* 3'UTR. Expression of Roquin-1 is assessed by GFP fluorescence, whereas that of *Tnf* 3'UTR is assessed by human CD4 reporter.

(G) Quantification of human CD4 (HuCD4) reporter (normalized to empty vector) on NIH 3T3 cells transduced with *Rc3h1^{WT}* or *Rc3h1^{SAN}* with *Tnf* 3'UTR. The vertical axis shows the fold difference in HuCD4 expression on NIH 3T3 cells transduced with either *Rc3h1^{WT}* or *Rc3h1^{SAN}* relative to empty vector. Data are representative of three independent experiments. Each column represents the mean of three replicates, and error bars represent SD. *p ≤ 0.05; **p ≤ 0.01.

(H) Representative plots of mock PBS- (left top panel) and LPS-injected (bottom left panel) mice showing TNF and CD11b staining and proportion of TNF⁺ cells among total splenic CD11b⁺ macrophages (middle panel) and TNF MFI on CD11b⁺ cells (right panel) from *Rc3h2^{+/+}* and *Rc3h2^{rin/rin}* mice 48 hr after 2.5 µg/g body weight LPS injection. Splenocytes were restimulated ex vivo with 100 ng/mL LPS in the presence of GolgiStop for 4 hr prior to intracellular TNF staining. Each dot represents an individual mouse, and bars represent median values in each group. *p ≤ 0.05.

(I) TNF production by *Rc3h2^{+/+}* or *Rc3h2^{rin/rin}* MEFs after 16 hr culture with 10 µg/mL LPS (measured in culture supernatants; left panel). Each dot represents a biological replicate, and columns represent median. ***p ≤ 0.001. Data are representative of three independent experiments. *Tnf* mRNA transcripts (normalized to β-actin) are measured by quantitative RT-PCR (right panel). Each column represents the mean of three technical replicates, and error bars represent SD. ***p ≤ 0.001. a.u., arbitrary unit. See also Figure S5.

Rc3h1^{ringless} T cells provided that there is normal Roquin-2, but this is impaired when the RING domain of Roquin-2 is also mutated. Hence the simplest explanation for the loss of *Icos* repression caused by the *Rc3h1*^{san} mutation, despite the presence of normal Roquin-2 in SGs, is that the ROQ-domain mutant protein still occupies its niche within these subcellular compartments and blocks the opportunity for functional compensation by Roquin-2. Similar differences between recessive null mutants and niche-filling loss-of-function point mutants have been described for other proteins that are members of potentially redundant families of paralogs, such as the MAP kinases in yeast (Madhani et al., 1997) and the IKAROS transcription factor family in mice (Papathanasiou et al., 2003).

In this study, both tagged and untagged full-length Roquin-1 protein failed to localize normally to SGs, defined either by eIF3 or TIA-1 markers, when the RING domain was selectively eliminated. Because the RINGLESS mutation has very similar in vivo consequences to complete loss of the Roquin-1 protein, the defect in SG localization is a clear and important finding of the current study because it demonstrates a striking correlation between Roquin-1 function and localization. As discussed above, it may explain why the Roquin-1^{RINGLESS} mutant is more effectively compensated by Roquin-2 than the Roquin-1^{SAN} mutant. It is interesting to compare the failure of the RINGLESS (133-1130) protein to localize to SGs with our earlier finding that fragments of Roquin-1 (138-337 or 138-484) that lacked both the RING domain and the C-terminal half of the protein could localize to SGs. This suggests that SG localization driven by the ROQ-CCCH domains is regulated by interplay between the N-terminal RING domain and the C-terminal domains that contain numerous potential sites for protein-protein interaction.

It is possible that the inability of Roquin-1^{RINGLESS} to localize to SGs is not in itself the direct cause of failed ICOS repression, given that *Icos* mRNA is found in SGs and also in P bodies (Yu et al., 2007) and *Icos* mRNA decay occurs in P bodies (Glasmacher et al., 2010). Indeed, Roquin-1^{RINGLESS} was found in P bodies when overexpressed in HEK293T cells. Instead, failure to localize to SGs may simply be an indicator of a severe functional defect in the protein. It is also possible that RNA-regulating processes in P bodies may be perturbed following defects in RNA-sorting pathways including impaired shuttling of RNA-binding proteins between SGs and P bodies.

ICOS expression, Tfh, and GC B cell numbers were still higher in *Rc3h1*^{san/san} mice than in double Roquin-1 and Roquin-2 *Tringless* mice. There are several nonmutually exclusive explanations for this observation. First, it is possible that either one or both the RING mutant proteins have not completely lost the RNA-regulating activity; this is particularly plausible in the case of Roquin-2 given the reported early lethality of *Rc3h2*^{-/-} mice (V. Heissmeyer, personal communication), which differs from our *Rc3h2*^{rin/rin} mice that are viable and healthy. Second, the ROQ mutant's actions in nonlymphoid cells, such as those in myeloid cells shown here, may exacerbate the T and B cell phenotypes. It is also possible that, at least in the regulation of some targets, Roquin-1^{SAN} exerts antimorphic effects—i.e., new or interfering activities that do not reflect the normal function of Roquin-1. Although this was not obvious in the case of ICOS regulation, Roquin-1^{SAN} appeared to aberrantly stabilize *Tnf*

mRNA. In support of this hypothesis, we have shown previously that Roquin-1^{SAN} binds *Icos* mRNA with 3-fold higher affinity than Roquin-1^{WT} in vitro (Athanasopoulos et al., 2010). Finally, the absence of perinatal lethality or vertebral malformation in *Rc3h1*^{san/san} homozygotes indicates that the ROQ domain mutation disrupts *Icos* (and *Tnf*) repression but preserves an apparently independent Roquin-1 activity in embryonic development that requires the RING domain.

The experiments here reveal that although Roquin-1 and Roquin-2 share some functional redundancies, their activities are not completely overlapping. This conclusion is based on the exaggerated TNF production by *Rc3h2*^{rin/rin} macrophages and MEFs with normal Roquin-1 and the lethal inflammatory disease and LPS-induced shock when the *Rc3h2*^{ringless} mutation was combined with *Rc3h1*^{san/san}. Roquin-1 and Roquin-2 may play nonredundant roles either by acting on the same mRNA targets (for example, *Tnf*) in different cell types and/or by acting on different mRNA targets within the same cell. In T cells, Roquin-1 plays the major role in the repression of ICOS based on the data from *Rc3h1*^{san/rin} compound heterozygous mice, and because a subtle phenotype is already observed in mice lacking active Roquin-1 (shown here for Roquin-1 *Tringless* mice and by Bertossi et al. [2011], by using T cell conditional *Rc3h1*^{-/-} mice) that is not fully compensated by Roquin-2. Roquin-1 also facilitates perinatal survival in a manner dependent on the RING domain, which cannot be either compensated by Roquin-2. These differences between Roquin-1 and Roquin-2 are likely to be mediated by their dissimilar C-termini that provide many sites for protein-protein interaction.

This study provides evidence of a role for Roquin-1 in non-T cells to alter the innate response to autoantibodies and bacterial lipopolysaccharide (LPS). In the K/BxN model of rheumatoid arthritis, immune complexes involving autoantibodies activate macrophages, neutrophils, and mast cells to secrete IL-1 β and TNF, which trigger a cascade of events leading to joint destruction (Ji et al., 2002; Lee et al., 2002). We have shown that the threshold for autoantibody-mediated arthritis is lowered as a direct consequence of the effect of Roquin-1^{SAN} on myeloid cells even in the absence of lymphocytes. This cell-intrinsic effect was confirmed by demonstrating that homozygosity for the “san” allele of *Rc3h1* accentuates septic shock as a result of TNF secretion by macrophages: *Rc3h1*^{san/san} mice succumbed to sublethal doses of LPS in a septic shock model that is dependent on TNF. Recent studies show an increasingly important contribution of myeloid cells (mainly macrophages and neutrophils) and TNF to lupus nephritis (Orme and Mohan, 2012; Saxena et al., 2011). It is therefore likely that the severe kidney damage in the *Rc3h1*^{san/san} *Rc3h2*^{rin/rin} mice is mediated by excessive TNF production.

Tnf mRNA decay has been known to be regulated by proteins that localize in SGs and bind *Tnf* 3'UTR (Carballo et al., 1998). The data here add to evidence from TTP-deficient mice (Taylor et al., 1996) and *TNF* transgenics that loss of strict posttranscriptional control of TNF is sufficient to cause arthritis. The functional hierarchy or relationship between Roquin-1, Roquin-2, and other *Tnf* mRNA regulators such as TIA-1 and TTP still needs to be elucidated. The RC3H family therefore emerges as a key player of posttranscriptional regulation of adaptive humoral immunity and the innate inflammatory response.

EXPERIMENTAL PROCEDURES

Mice and Immunizations

Roquin-1 *ringless* and Roquin-2 *ringless* mice were generated by Ozgene, *LoxP* sites that flanked or “floxed” *Rc3h1/2* exon 2, encoding the start codon and RING motif were introduced via homologous recombination in C57BL/6 mouse embryonic stem cells (ESCs). Recombinant ESC clones were implanted into foster mothers to yield chimeras. Heterozygote progeny were screened for germline transmission before crossing to *Rosa26-Flp1* mice to remove the *Neo^r* cassette. Floxed *Rc3h1* and *Rc3h2* heterozygotes (*Rc3h2^{fllox/+}*) were then crossed to mice expressing *cre* under the control of the endogenous *Rosa26* promoter. Removal of *cre* expression by backcrossing to C57BL/6 yielded germline deletions of *Rc3h1/2* exon 2 (Roquin-1/Roquin-2 *ringless* [*rin* allele]). C57BL/6 *Tnf^{-/-}* mice were made by H. Korner. *Rc3h1^{san}* mice were generated as previously described (Vinueza et al., 2005). Mice were housed under specific pathogen-free conditions. Where indicated, 8- to 12-week-old mice were immunized intraperitoneally (i.p.) with 2×10^9 SRBC to generate a GC response. To assess TNF production, we injected mice i.p. with LPS, and spleens were harvested 48 hr postinjection. All experiments were approved by the Australian National University Animal Ethics and Experimentation Committee.

Plasmid Construction

To construct the N-terminal V5 tagged full-length Roquin-1, we PCR amplified the cDNA from plasmid *Roquin-GFP3* by using primers Roquin1F1: 5'-GGCTCTAGAATTCGCAATGCCCTGTACAAGCTCC-3' and SR-DownNotI: 5'-CGCGAATGCGGCCGCCGGGAGCAGAATTGGAAACAAC-3'. The amplicon was cloned into the EcoRI-NotI sites of the entry vector pENTR3C (Invitrogen). This was recombined into the destination vector pcDNA3.1/nV5-DEST (Invitrogen). The RINGLESS version of Roquin-1 was generated by using site-directed mutagenesis (Quikchange, Agilent Technologies) to create a second EcoRI site immediately upstream of the ATG codon at amino acid position 133 (5'-ACTACTCAGAGT GTTCTGGAATCCCAATGCAGAG GAAACTT-3') in the full-length Roquin-1 pENTR3C clone described above. This construct was cut by using EcoRI to excise the RING domain region and the vector religated. The resulting pENTR3C construct was recombined into the destination vector pcDNA3.1/nV5-DEST (Invitrogen) generating V5-*Rc3h1^{RINGLESS}*. The untagged Roquin-1^{RINGLESS} retroviral construct was constructed by cutting the Roquin-1^{RINGLESS} pENTR3C vector Sall and EcoRV and subcloned into the XhoI-blunted EcoRI sites of pKMV. The N-terminal V5-tagged human RC3H2 cDNA was subcloned from MNAB-GFP (Athanasopoulos et al., 2010) as an XbaI-NotI fragment and cloned into the same sites of pBluescriptII SK+. The fragment was excised using BamHI-NotI and cloned into the same sites of pENTR2B before recombination into pcDNA3.1/nV5-DEST by using the Gateway recombination system (Invitrogen). To construct the C-terminal FLAG-tagged Roquin-1, we excised the cDNA from plasmid *Roquin-GFP* (Athanasopoulos et al., 2010) and cloned it into the XbaI-NotI sites of the vector pMZSF3 (kind gift from J.F. Greenblatt, University of Toronto).

Antibodies

Antibodies for immunofluorescence studies were as follows: DCP1A (gift from J. Lykke-Andersen, University of California San Diego), eIF3 (Santa Cruz Biotechnology), V5-tag (AbD Serotec), FLAG-tag (Sigma-Aldrich), rabbit anti-sera against Roquin-2 (gift from Steven Hefeneider; Oregon Health and Science University), and Roquin-1 (Novus Biologicals). Secondary antibodies were conjugated to Alexa 568 or Alexa 488 (Molecular Probes, Invitrogen). Antibodies for flow cytometric studies were as follows: mouse CD4, B220, CD11c, CXCR5, CD25, GL-7, Fas (CD95), and human CD4 were purchased from BD Biosciences; mouse CD11b and CD44 were purchased from BioLegend; and mouse PD-1, ICOS, and TNF were purchased from eBioscience.

Flow Cytometry

Lymph nodes and spleen for myeloid cell population analysis were treated with Collagenase P (Roche) and DNase I (Sigma-Aldrich) before preparing single-cell suspensions. To stain for surface markers, we incubated cells in the antibody mixture diluted in ice-cold staining buffer (2% fetal calf serum [FCS] and 0.1% Na₂S₂O₃ in PBS). Intracellular TNF was stained by using the Intracellular

Staining Kit (eBioscience). Cytokines in culture supernatants and serum were measured by using CBA bead assays following the manufacturer's instructions (BD Biosciences). A BD FACSCalibur and LSRII Flow Cytometer with FACSDiva software were used for flow cytometry acquisition, and FlowJo (Tree Star) was used for analysis.

In Vitro LPS Stimulation and Cytokine Measurements

For measurements of TNF from culture supernatants, peritoneal cells (5×10^5 /well) from mice injected 6 days previously with 100 μ l of K/BxN serum were stimulated with 1 μ g/ml *E. coli* LPS (Sigma-Aldrich). Culture supernatants were collected after a 5-day incubation period. *Rc3h2^{rin/rin}* and *Rc3h2^{+/+}* fibroblasts were isolated from E14 embryos, cultured in DMEM medium supplemented with 10% FCS and antibiotics, and stimulated with 10 μ g/ml LPS for 16 hr. The Mouse Inflammation Cytokine Bead Array kit (BD Biosciences) was used to determine TNF concentrations. Intracellular TNF measurement was performed after overnight stimulation with 100 ng/ml *E. coli* LPS.

Immunofluorescence

HEK293T cells were prepared for fluorescence microscopy as previously described (Athanasopoulos et al., 2010). Images were collected by using an Olympus IX71 microscope with DP Controller software (Olympus) and compiled by using Adobe Photoshop software.

KBxN Serum-Induced Arthritis

C57BL/6 *Rag1^{-/-} Rc3h1^{san/san}* or *Rag1^{-/-} Rc3h1^{+/+}* control littermates were injected intravenously with pooled serum obtained from arthritic K/BxN mice. Criteria for clinical scores were as follows: 0, normal; 1, mild swelling of the dorsum of paw; 2, mild redness and swelling of one large joint or redness and swelling limited to individual digits (any number of digits); 3, redness and swelling of two large joints, or severe redness and swelling of entire paw (including digits); 4, maximally inflamed limb with involvement of multiple joints. Scores for each limb were added. Ankle thickness was measured with an electronic calliper.

Endotoxic Shock Induction

Susceptibility to LPS plus D-galactosamine was examined by intravenously (i.v.) injection of 20 mg D-galactosamine (Sigma-Aldrich) and 5 pg/g LPS (Sigma-Aldrich) into *Rag1^{-/-} Rc3h1^{san/san}* or *Rag1^{-/-} Rc3h1^{+/+}* controls. This sublethal dose was selected after titration of susceptibility to LPS plus D-gal in *Rag1^{-/-}* mice. Mice were closely monitored for any signs of septic shock and sacrificed at 72 hr.

Retroviral Transductions

Packaging of retroviruses, virus titrations, transduction of NIH 3T3 cells, and quantification of target mRNA expression relative to empty vector expression have been described before (Vinueza et al., 2005; Yu et al., 2007). The full-length or CDS of *Icos* mRNA and 3'UTR of *Tnf* mRNA (clone NM_013693.2) were amplified by PCR and inserted into the *pR-IRES-CD4* retroviral vector. *Rc3h1* and *RC3H2* cDNA were also amplified and inserted into the *pR-IRES-GFP* retroviral vector. Primer sequences are available on request. Retroviral supernatants were harvested from packaging Phoenix cells transfected with individual retroviral constructs. NIH 3T3 cells were transduced by retroviruses via spinoculation.

Immunoprecipitation and Immunoblotting

Whole-cell lysates were prepared using TNE lysis buffer (1% NP-40, 150 mM NaCl, 20 mM Tris-base, 1 mM EDTA and Roche Complete EDTA-free protease inhibitory cocktail tablet). To immunoprecipitate proteins, we added antibody to precleared lysates, mixed them with Protein G Sepharose 4 Fast Flow (GE Healthcare) for 12 hr, and then washed them. For immunoblotting, lysates were separated by SDS-PAGE, transferred to nitrocellulose membrane, blocked in 5% BSA Tris-buffered saline containing 0.05% Tween-20, probed with primary antibodies, and detected with horseradish peroxidase-conjugated anti-rabbit secondary antibodies.

Histology

Tissues were fixed in 10% neutral buffered formalin and embedded in paraffin. We stained 100 μ m thick sections with H&E or Luxol Fast Blue-Cresyl Violet

(LFB-CV) where indicated. For evaluation of arthritis, H&E staining was performed on paraffin-embedded knee-joint sections taken 6 days after 200 μ l K/BxN serum transfer. The F4/80 antibody used in the immunohistochemical staining of knee joint was purchased from BioLegend.

Quantitative PCR

Real-time PCR reactions were performed following standard protocols previously described (Vinuesa et al., 2005). In brief, RNA was isolated by using TRIzol reagent (Invitrogen) and reverse-transcribed with oligo(dT) by using Superscript II RT enzyme (Invitrogen). cDNA expression was determined with the ABI Prism 7900 sequence detection system and Sybr-Green reagents (Applied Biosystems). Primer sequences for *Il1b* and *Tnf* are available on request. Fluorescence signals were measured over 40 PCR cycles and the cycle (*Ct*) at which signals crossed a threshold set within the logarithmic phase was recorded. The *Ct* for the target gene was subtracted from the *Ct* for β -actin (ΔC_t). The relative amount of mRNA was calculated as $2^{-\Delta C_t}$.

Statistical Analysis

Statistics were calculated by nonparametric Mann-Whitney test (U test) to analyze two variable comparisons in flow cytometry experiments and when assessing arthritis scores over time. Results from cell culture experiments were analyzed by using unpaired Student's t test. All statistical analysis was performed with Prism software (GraphPad Software). Statistically significant differences are indicated as * = $p \leq 0.05$, ** = $p \leq 0.01$, *** = $p \leq 0.001$, and ns = not significant. Unless otherwise specified, each dot in graphs corresponds to one biological replicate.

SUPPLEMENTAL INFORMATION

Supplemental Information includes five figures and Supplemental Experimental Procedures and can be found with this article online at <http://dx.doi.org/10.1016/j.immuni.2013.01.011>.

ACKNOWLEDGMENTS

We thank Professor Paul Waring and the Australian Phenomics Network, University of Melbourne, for the histopathology analysis of the *Rc3h1^{san/san}Rc3h2^{rin/rin}* mice. We thank Anne Prins for histology slides preparation. We thank the ACRF Biomolecular Resource Facility and the Microscopy and Cytometry Resource Facility, John Curtin School of Medical Research for technical support. This work was funded by an Elizabeth Blackburn NH&MRC Senior Research Fellowship to C.G.V. and NH and MRC program and project grants to C.G.V., M.C.C. and C.C.G.

Received: August 20, 2012
Accepted: January 28, 2013
Published: April 11, 2013

REFERENCES

- Athanasopoulos, V., Barker, A., Yu, D., Tan, A.H., Srivastava, M., Contreras, N., Wang, J., Lam, K.P., Brown, S.H., Goodnow, C.C., et al. (2010). The ROQUIN family of proteins localizes to stress granules via the ROQ domain and binds target mRNAs. *FEBS J.* **277**, 2109–2127.
- Bertossi, A., Aichinger, M., Sansonetti, P., Lech, M., Neff, F., Pal, M., Wunderlich, F.T., Anders, H.J., Klein, L., and Schmidt-Supprian, M. (2011). Loss of Roquin induces early death and immune deregulation but not autoimmunity. *J. Exp. Med.* **208**, 1749–1756.
- Carballo, E., Lai, W.S., and Blakeshear, P.J. (1998). Feedback inhibition of macrophage tumor necrosis factor- α production by tristetraprolin. *Science* **281**, 1001–1005.
- Chang, P.P., Lee, S.K., Hu, X., Davey, G., Duan, G., Cho, J.H., Karupiah, G., Sprent, J., Heath, W.R., Bertram, E.M., and Vinuesa, C.G. (2012). Breakdown in repression of IFN- γ mRNA leads to accumulation of self-reactive effector CD8+ T cells. *J. Immunol.* **189**, 701–710.
- Glasmacher, E., Hoefig, K.P., Vogel, K.U., Rath, N., Du, L., Wolf, C., Kremmer, E., Wang, X., and Heissmeyer, V. (2010). Roquin binds inducible costimulator mRNA and effectors of mRNA decay to induce microRNA-independent post-transcriptional repression. *Nat. Immunol.* **11**, 725–733.
- Ji, H., Ohmura, K., Mahmood, U., Lee, D.M., Hofhuis, F.M., Boackle, S.A., Takahashi, K., Holers, V.M., Walport, M., Gerard, C., et al. (2002). Arthritis critically dependent on innate immune system players. *Immunity* **16**, 157–168.
- Kedersha, N., Stoecklin, G., Ayodele, M., Yacono, P., Lykke-Andersen, J., Fritzier, M.J., Scheuner, D., Kaufman, R.J., Golan, D.E., and Anderson, P. (2005). Stress granules and processing bodies are dynamically linked sites of mRNP remodeling. *J. Cell Biol.* **169**, 871–884.
- Korganow, A.S., Ji, H., Mangialaio, S., Duchatelle, V., Pelanda, R., Martin, T., Degott, C., Kikutani, H., Rajewsky, K., Pasquali, J.L., et al. (1999). From systemic T cell self-reactivity to organ-specific autoimmune disease via immunoglobulins. *Immunity* **10**, 451–461.
- Lee, D.M., Friend, D.S., Gurish, M.F., Benoist, C., Mathis, D., and Brenner, M.B. (2002). Mast cells: a cellular link between autoantibodies and inflammatory arthritis. *Science* **297**, 1689–1692.
- Lee, S.K., Silva, D.G., Martin, J.L., Pratama, A., Hu, X., Chang, P.-P., Walters, G., and Vinuesa, C.G. (2012). Interferon- γ excess leads to pathogenic accumulation of follicular helper T cells and germinal centers. *Immunity* **37**, 880–892.
- Linterman, M.A., Rigby, R.J., Wong, R.K., Yu, D., Brink, R., Cannons, J.L., Schwartzberg, P.L., Cook, M.C., Walters, G.D., and Vinuesa, C.G. (2009). Follicular helper T cells are required for systemic autoimmunity. *J. Exp. Med.* **206**, 561–576.
- Madhani, H.D., Styles, C.A., and Fink, G.R. (1997). MAP kinases with distinct inhibitory functions impart signaling specificity during yeast differentiation. *Cell* **91**, 673–684.
- Matsumoto, I., Staub, A., Benoist, C., and Mathis, D. (1999). Arthritis provoked by linked T and B cell recognition of a glycolytic enzyme. *Science* **286**, 1732–1735.
- Ohlsson, K., Björk, P., Bergenfeldt, M., Hageman, R., and Thompson, R.C. (1990). Interleukin-1 receptor antagonist reduces mortality from endotoxin shock. *Nature* **348**, 550–552.
- Orme, J., and Mohan, C. (2012). Macrophages and neutrophils in SLE-An online molecular catalog. *Autoimmun. Rev.* **11**, 365–372.
- Papathanasiou, P., Perkins, A.C., Cobb, B.S., Ferrini, R., Sridharan, R., Hoyne, G.F., Nelms, K.A., Smale, S.T., and Goodnow, C.C. (2003). Widespread failure of hematolymphoid differentiation caused by a recessive niche-filling allele of the Ikaros transcription factor. *Immunity* **19**, 131–144.
- Peschon, J.J., Torrance, D.S., Stocking, K.L., Glaccum, M.B., Otten, C., Willis, C.R., Charrier, K., Morrissey, P.J., Ware, C.B., and Mohler, K.M. (1998). TNF receptor-deficient mice reveal divergent roles for p55 and p75 in several models of inflammation. *J. Immunol.* **160**, 943–952.
- Saxena, R., Mahajan, T., and Mohan, C. (2011). Lupus nephritis: current update. *Arthritis Res. Ther.* **13**, 240–251.
- Siess, D.C., Vedder, C.T., Merckens, L.S., Tanaka, T., Freed, A.C., McCoy, S.L., Heinrich, M.C., Deffebach, M.E., Bennett, R.M., and Hefeneider, S.H. (2000). A human gene coding for a membrane-associated nucleic acid-binding protein. *J. Biol. Chem.* **275**, 33655–33662.
- Solomon, S., Rajasekaran, N., Jeisy-Walder, E., Snapper, S.B., and Illges, H. (2005). A crucial role for macrophages in the pathology of K/B x N serum-induced arthritis. *Eur. J. Immunol.* **35**, 3064–3073.
- Taylor, G.A., Carballo, E., Lee, D.M., Lai, W.S., Thompson, M.J., Patel, D.D., Schenkmann, D.I., Gilkeson, G.S., Broxmeyer, H.E., Haynes, B.F., and Blakeshear, P.J. (1996). A pathogenetic role for TNF α in the syndrome of cachexia, arthritis, and autoimmunity resulting from tristetraprolin (TTP) deficiency. *Immunity* **4**, 445–454.
- Vinuesa, C.G., Cook, M.C., Angelucci, C., Athanasopoulos, V., Rui, L., Hill, K.M., Yu, D., Domaschenz, H., Whittle, B., Lambe, T., et al. (2005). A RING-type ubiquitin ligase family member required to repress follicular helper T cells and autoimmunity. *Nature* **435**, 452–458.
- Yu, D., Tan, A.H., Hu, X., Athanasopoulos, V., Simpson, N., Silva, D.G., Hutloff, A., Giles, K.M., Leedman, P.J., Lam, K.P., et al. (2007). Roquin represses autoimmunity by limiting inducible T-cell co-stimulator messenger RNA. *Nature* **450**, 299–303.